Stable Acinar Progenitor Cell Model Identifies Treacle-Dependent Radioresistance

Authors: Thomas J. Weber, Wei-Jun Qian, Jordan N. Smith, Marina A. Gritsenko, Dehong Hu, et. al.

Source: Radiation Research, 192(2) : 135-144

Published By: Radiation Research Society

URL: https://doi.org/10.1667/RR15342.1

RADIATION RESEARCH **192**, 135–144 (2019)
0033-7587/19 $15.00

DOI: 10.1667/RR15342.1

Stable Acinar Progenitor Cell Model Identifies Treacle-Dependent Radioresistance

Thomas J. Weber,[a,1] Wei-Jun Qian,[b] Jordan N. Smith,[a] Marina A. Gritsenko,[b] Dehong Hu,[c] William B. Chrisler[a] and Charles Timchalk[a]

[a] *Health Impacts and Exposure Science Group,* [b] *Integrative Omics Group and* [c] *Environmental Molecular Sciences Laboratory, Pacific Northwest National Laboratory, Richland, Washington 99352*

Weber, T. J., Qian, W-J., Smith, J. N., Gritsenko, M. A., Hu, D, Chrisler, W. B. and Timchalk, C. Stable Acinar Progenitor Cell Model Identifies Treacle-Dependent Radioresistance. *Radiat. Res.* 192, 135–144 (2019).

Radiotherapy for head and neck cancers can result in extensive damage to the salivary glands, significantly affecting patient quality of life. However, the salivary gland can recover in patients receiving lower doses of radiation. In addition, there is considerable interest in delineating the mechanisms by which stem cells survive radiation exposure and promote tissue regeneration. In this study, we isolated stable radioresistant acinar progenitor cells from the submaxillary gland of the Sprague Dawley rat. Progenitor cells are characterized as c-Kit^{high}/alpha-amylase^{+} and are resistant to X rays (≤5 Gy). We further isolated a radiosensitive acinar counterpart, characterized as c-Kit^{low}/alpha-amylase^{+}, which is effectively killed by exposure to 2 Gy X ray of radiation. Phosphopeptides with homology to the treacle protein (TCOF1) were disproportionately increased in progenitor cells, compared to their radiosensitive counterparts. Silencing of TCOF1 expression (shRNA) radiosensitized progenitor cells, a response conserved in human cells with TCOF1 knockdown. Collectively, these observations indicate that radiation resistance is an intrinsic property of c-Kit^{high} salivary gland progenitor cells. Since human salivary gland stem cells with c-Kit expression are believed to have enhanced regenerative potencies, our model system provides a stable platform to investigate molecular features associated with c-Kit expression that may contribute to protection or stabilization of the stem cell niche.

INTRODUCTION

The goal of this work was to establish a new cellular model system for investigating conserved molecular mechanisms of radiation resistance in salivary gland stem/progenitor cells. Head and neck cancers account for ≈4% of all cancers in the U.S. and estimates indicate that >64,000 people will die from head and neck cancers this year (*1*). Due to the location of many oral tumors, radiotherapy of head and neck cancers often results in extensive damage to the salivary glands. The salivary glands play critical roles in food digestion, oral mucosal protection, remineralization of dental tissues and moistening of the palate for articulation (*2*). Damage to the salivary glands results in a number of adverse side effects, including xerostomia, difficulty swallowing, oral discomfort, malnutrition, oral mucositis, changes in taste and increased oral infections (*3–5*). At worst, destruction of oral tissues by radiotherapy can lead to morbidity (*2*).

Salivary glands, which are highly sensitive to radiation, are unique relative to other radiosensitive tissues, because the cells of the salivary gland proliferate slowly and are highly differentiated (*6*). Within the first week of radiotherapy, affected individuals can experience a 50–60% loss of salivary flow (*7*), which is accompanied by loss of acinar cells and glandular shrinkage (*8, 9*). Acute salivary gland damage may also contribute to radiation-induced chronic tissue effects characterized by decreased or non-stimulated salivary flow (*10, 11*). Importantly, patients who received lower doses of radiation have shown recovery of salivary gland function between 12–24 months (*11, 12*). This indicates that salivary gland stem cells capable of surviving radiation exposure (up to some defined dose) retain the capacity to regenerate damaged tissue. This suggestion is consistent with the characterizations of stem and progenitor cells as radioresistant phenotypes (*13, 14*). Thus, there is considerable interest in the cellular and molecular mechanisms by which stem/progenitor cells defend themselves against radiation.

Animal models used to investigate the salivary gland acute phase response have shown consistent reductions in salivary flow rate, loss of glandular weight and loss of acinar area (*2*). Therefore, salivary gland stem/progenitor cells derived from animal models can provide opportunities to better understand the conserved cellular and molecular

Editor's note. The online version of this article (DOI: 10.1667/RR15342.1) contains supplementary information that is available to all authorized users.

[1] Address for correspondence: 902 Battelle Blvd., J4-02, Pacific Northwest National Laboratory, Richland, WA 99354; email: Thomas.Weber@pnnl.gov.

mechanisms underlying radiation resistance that contribute to tissue regeneration. The development of methods to enable salivary gland stem cells to survive radiation and effect tissue repair could lead to a reduction in adverse side effects of radiation associated with head and neck cancers. Alternatively, with the use of transplanted stem cells, independent investigators have shown great promise in recovering damaged salivary gland function in mice (*15*). In particular, human salivary gland stem cells positive for c-Kit expression have shown enhanced regenerative potencies (*16*). Initial attempts to use autologous salivary stem cells to re-populate damaged salivary glands in affected individuals was hindered by an inability to maintain the stem cell phenotype for prolonged periods *in vitro* (*2*). In more recently reported advances, the long-term culture of salivary gland stem cells has been addressed to overcome this hurdle (*17*). In contrast to human stem cells, those that are isolated from animal models, including rodent salivary gland stem cells, often display a relatively stable phenotype *in vitro* (*15*). The stability of stem cells derived from animals is an attractive feature that can enable detailed investigation of the conserved cellular and molecular mechanisms contributing to radiation resistance and tissue regeneration.

In the current study we provide experimental evidence for a new stable acinar progenitor model system to investigate molecular mechanisms of radioresistance. Our model is comprised of radioresistant and radiosensitive acinar cells isolated from the submaxillary gland of the Sprague Dawley® rat, which exhibits a stable phenotype *in vitro* (*18, 19*). We anticipate that this model system will enable detailed mechanistic studies of radioresistance mechanisms that are conserved in human and rat salivary gland stem/progenitor cells. In support of this statement, we identify a role for the treacle protein (TCOF1) as a mediator of radioresistance in rat salivary gland progenitor cells, and TCOF1 is a known mediator of radioresistance in human cells (*20*). Thus, molecular mechanisms of radioresistance conserved in human cells are apparent and it is anticipated that additional conserved features of radioresistance can be identified using this model system.

MATERIALS AND METHODS

Isolation and Culture of Primary Cells from the Rat Submaxillary Gland

A detailed protocol for the isolation of primary cells from the rat submaxillary gland can be found in the supplementary material of our previously published work (*18*). The mixed population of primary cells (epithelial, endothelial, stromal) isolated from the submaxillary gland were maintained in advanced DMEM:F12 (Thermo Fisher Scientific™ Inc., Waltham, MA) supplemented with 2% fetal bovine serum (FBS), 10 ng/ml epidermal growth factor (EGF), 2 m*M* GlutaMAX™, 100 units/ml penicillin, 100 units/ml streptomycin, 0.25 μg/ml fungizone. In select experiments, cells were maintained in the original DMEM:F12 formula (Thermo Fisher Scientific) containing the same supplements, but with FBS concentrations increased to 10%, to determine whether proprietary/undefined components of the advanced DMEM:F12 media were inducing radioresistance. Both freshly prepared cells and cryopreserved stocks were used for experiments. Cryopreserved stocks are prepared when freshly isolated primary cells have formed small (10–20 cell) circular epithelial colonies, indicating that cells have recovered from the isolation protocol and have engaged in proliferation. Cell stocks containing mixed stromal/epithelial cell types from this first passage are cryopreserved for future use, and in some cases a brief trypsinization (0.05%, 2–4 min) is performed to remove stromal cells and enrich for epithelial cells prior to cyropreservation.

Isolation of Radioresistant and Sensitive Variants

Cells from the initial enzymatic digestion of the salivary gland or from first-passage cryopreserved stocks were established in T25 flasks until proliferation of epithelial cells was apparent. For flasks with visible numbers of stromal cells, a brief trypsinization (0.05% trypsin, 2–4 min) was performed to remove the stromal cells, followed by trypsinization with 0.25% trypsin to detach the epithelial cells. Cells were then seeded at very low density (~5 cells/35-mm dish) and maintained for ~5–7 days, at which time colonies arising from the clonal expansion of single cells could be discerned using phase contrast microscopy. For each dish, all but one colony was removed with a sterile cotton swab, as described elsewhere (*18*), with emphasis on preserving colonies with uniform epithelial morphology, which were identified as the radioresistant cell type in pilot studies (see Supplementary data, Fig. S1; http://dx.doi.org/10.1667/RR15342.1.S1). Dishes were then maintained for an additional 7 days to confirm the presence of a single colony, which was expanded into a cell line by standard subculture technique. Colonies with sufficient proliferative potential for experimental analysis, defined by the capacity to be passaged into multiple T75 flasks, were prioritized for follow-on investigation and stocks were cryopreserved to enable continued investigations using the same clonally-derived cell lines.

Fibroblast Cell Culture

Normal human dermal fibroblasts purchased from Lonza (Allendale, NJ) were maintained in either fibroblast growth media according to manufacturer's directions or advanced DMEM:F12 supplemented with 2% FBS, 2 m*M* GlutaMAX, 100 units/ml penicillin, 100 units/ml streptomycin, 0.25 μg/ml fungizone and 10 ng/ml basic fibroblast growth factor (bFGF). Fibroblasts were subcultured by trypsinization.

Irradiation

Cells were X-ray irradiated using the Therapax X-RAD 320 system equipped with a 320-kV high-stability X-ray generator, metal ceramic X-ray tube, variable X-ray beam collimator and no. 8 filter (operated at 300 kV for cell irradiation; dose rate = 1.68 Gy/min; Precision X-ray Inc., East Haven, CT). To verify dosimetry, OSL nanoDots™ and InLight dosimeters (Landaur® Inc., Glenwood, IL) were placed underneath a dish containing cells exposed to 10 Gy of X-ray radiation. Chips were read twice and averaged by the Pacific Northwest National Laboratory's Radiation Protection Program, and results were confirmed independently by Landaur, Inc.

Clonogenic Survival

Cells were trypsinized and passed through a 70-μm nylon mesh. Cell number was then quantified using a Coulter Counter®, and an equal number of cells were seeded into culture dishes (1,000 cells/10-cm dish; 150 cells/6-cm dish). At 24 h after plating, cells were irradiated, and immediately after irradiation media was replaced with fresh growth media. Clonogenic survival assay was performed as described elsewhere (*21*) with the following modifications. Colonies (≥50 cells) were typically quantified starting at day 7 postirradiation (control and radiation doses ≤5 Gy), with high-dose radiation groups (>5 Gy) maintained in culture for up to 14 days, with cultures

monitored daily and media changed at 3-day intervals. This time extension was necessary to improve the accuracy of colony counts because high doses induced a significant delay in proliferation, which translated to decreased colony number on day 7 compared to days 8–14. The criteria for terminating the clonogenic survival assay in high-dose radiation groups was simply identifying whether colonies reached very large sizes (often nearing the point of coming into contact with each other) or whether colonies showed no sign of growth between days 8–12, indicating permanent mitotic arrest. Initially, we investigated seeding densities of 1,000 cells/10-cm dish. The assay scaled accurately to 6-cm dishes seeding 150 cells/dish, which is now routinely used in experimental design. Clonogenic survival for fibroblasts was determined as described elsewhere (*22*).

Antibody-Based Detection Methods

Western blot and immunofluorescence analysis of cells were performed as described elsewhere (*18*). Antibodies included salivary amylase alpha (α-amylase; Novus Biologicals, Littleton, CO), aquaporin 5 (AQP5) and c-Kit (both acquired from Santa Cruz Biotechnology® Inc., Dallas, TX), TCOF1 (Proteintech® Group Inc., Rosemont, IL) and actin (Millipore, Temecula, CA). Final titers for primary antibodies were 1:3,000 and secondary antibodies were 1:5,000 (Thermo Scientific™, Rockford, IL). Click-iT EdU Imaging Kit with Alexa Fluor® 647 azide kit was used according to manufacturer's directions (Thermo Scientific). In select experiments the pIMAGO kit (Tymora Analytical Operations, West Lafayette, IN) was used to assess the phosphorylation status of immunoprecipitated proteins according to manufacturer's directions.

Microarray

Three independent radioresistant cell lines (clones 4, 5 and 10; derived by the clonal expansion of single submaxillary gland epithelial cells) were analyzed using microarray. Rat expression microarray analysis (ArrayStar Inc., Rockville, MD) was completed. Total RNA from each sample was quantified using the NanoDrop ND-1000 and the RNA integrity was assessed by standard denaturing agarose gel electrophoresis. For microarray analysis, the Agilent Array platform was employed (Santa Clara, CA). The sample preparation and microarray hybridization were performed based on the manufacturer's standard protocols. Briefly, total RNA from each sample was amplified and transcribed into fluorescent cRNA using the Agilent Technology Quick Amp Labeling version 5.7 protocol. The labeled cRNAs were hybridized onto the Whole Rat Genome Oligo Microarray (4×44 K; Agilent Technologies). After the slides were washed, the arrays were scanned using an Agilent Scanner G2505C. Agilent Feature Extraction software version 11.0.1.1 was used to analyze acquired array images. Quantile normalization and subsequent data processing were performed using the GeneSpring GX version 12.1 software (Agilent Technologies). After quantile normalization of the raw data, genes that were consistently expressed in all three cell lines were evaluated to identify the radioresistant cell type.

Quantitative Phosphoproteomics. Protein Digestion and 8-Plex iTRAQ Labeling of Peptides

Cell pellets were lysed in 100 µl lysis buffer containing 8 *M* urea, 75 m*M* NaCl in 100 m*M* NH_4HCO_3 (pH 7.8), 10 m*M* NaF, phosphatase inhibitor cocktails 2 and 3 (both acquired from MilliporeSigma, St. Louis, MO) and the cOmplete™ ULTRA protease inhibitor (Roche Molecular Systems Inc., Pleasanton, CA). Protein concentrations were determined using BCA assay. Proteins were reduced with 5 m*M* dithiothreitol for 1 h at 37°C, and were subsequently alkylated with 10 m*M* iodoacetamide. Samples were diluted twofold with 50 m*M* NH_4HCO_3 and digested with trypsin at a ratio of 1:50 trypsin:protein (w/w) for 4 h at 37°C, diluted by fourfold, and subjected to a second treatment with trypsin and incubation at room temperature overnight (~16 h). The digest was acidified with trifluoroacetic acid to pH ~2.5. Tryptic peptides were desalted on reversed phase C18 SPE columns (50 mg; Supelco Discovery®, Millipore Sigma) and dried using SpeedVac. Desalted peptides were labeled with 8-plex iTRAQ reagents according to the manufacturer's instructions (AB Sciex™, Framingham, MA). Peptides (100 µg) from each sample were dissolved in 30 µl of 0.5 *M* triethylammonium bicarbonate (pH 8.5) solution and labeling reagent in 70 µl of ethanol was added for each channel. After 1-h incubation, 8 µl of 5% hydroxylamine was added to hydrolyze excess reagents for an additional 15-min incubation. Differential labeled peptides from all six channels (126, 127, 128, 129, 130, 131) were pooled, acidified by 10% TFA, and desalted again using C18 SPE columns.

Enrichment of phosphopeptides. iTRAQ-labeled peptides were subjected to immobilized metal affinity chromatography (IMAC) for phosphopeptide enrichment. Magnetic Fe^{3+}-NTA-agarose beads were prepared using the Ni-NTA-agarose beads (QIAGEN®, Valencia, CA) following the protocols reported elsewhere (*23*). Briefly, peptides (~100 µg) were reconstituted in 300 µl IMAC binding/wash buffer (80% MeCN, 0.1% TFA) and incubated for 30 min with 75 µl of the 5% bead suspension. After incubation, the beads were washed 4 times each with 300 µl of wash buffer. Phosphorylated peptides were eluted from the beads using 50–75 µl of 1:1 ratio of acetonitrile to 2.5 % ammonia in 2 m*M* (pH 8) phosphate buffer (v/v) after incubating for 1.5 min. Samples were acidified and concentrated, then were reconstituted to 30 µl with 0.1% TFA for LC-MS/MS analysis.

Mass spectrometry analysis. Data were acquired using a nano-ACQUITY UPLC® system (Waters® Corp., Milford, MA) coupled to an Orbitrap™ Lumos™ mass spectrometer (Thermo Scientific, San Jose, CA). Peptides were directly injected on a home-packed 75-µm i.d. × 20 cm analytical column (1.9 µm ReproSil C18) maintained at 50°C. Solvents used were 0.1% FA in water as mobile phase A and 0.1% FA in 90% ACN as mobile phase B. The gradient was as follows: 2–6% solvent B for 1 min, 6–30% solvent B for 84 min, 30–60% solvent B for 9 min, 60–90% solvent B for 1 min and finally 90% solvent B for 5 min. Flow was controlled at 200 nl/min. The mass spectrometer was operated in data-dependent mode. Full-scan MS spectra from m/z 350–1,800 were acquired at a resolution of 60,000 at m/z 400 after accumulation to a target value of 4×10^5. The cycle time was 2 s. HCD fragmentation was performed at normalized collision energy of 30% after the accumulation to a target value of 1×10^5. MS/MS was acquired at a resolution of 50,000.

Data analysis. MS/MS raw data were converted to .dta files using an in-house software DeconMSn. Peptides were identified from MS/MS spectra using database searching algorithm MS-GF+ version 9949 (*24*) against the human protein database downloaded (in April 2012) from Uniprot. Static modification of 8-plex iTRAQ (304.2053 Da) on lysine residue and N-termini of peptides, carbamidomethylation of cysteine residues (57.0215 Da) and dynamic oxidation of (15.9949 Da) methionine, and dynamic phosphorylation (79.966) on Ser/Thr/Tyr residues were applied during the database search. Both fully and partially tryptic peptides were considered with two missed cleavages allowed. The mass tolerance for precursor ions was 50 ppm and fragmentation tolerance for HCD was 0.05 Da. All peptides were identified with <0.1% false discovery rate using a MS-generating function score (MS-GF) < 1E–10 and a decoy database searching strategy (*25*). The reporter ion intensities for each channel in each biological condition were extracted using the MS/MS automated selected ion chromatogram (MASIC) generator (an in-house tool) for quantification. For a given protein, the reporter ion intensities in each channel were summed for all identified spectra. Statistical analysis of significance was performed using the DAnTE software tool (*26*) to identify proteins with significant abundance changes.

Fluorescence Imaging

Fluorescence imaging of progenitor cells was performed on an inverted fluorescence confocal microscope (Zeiss LSM 710 with

Airyscan; Carl Zeiss AG, Oberkochen, Germany). An oil immersion 100× NA1.46 objective was used to image the cells. Cell nuclei were stained with DAPI, which were detected by 405-nm wavelength laser excitation. TCOF1 foci were detected using anti-TCOF1 primary antibody and goat anti-rabbit-Alexa488 secondary using 488-nm wavelength laser excitation. The Zeiss Airyscan technology increases the spatial resolution of conventional diffraction-limited confocal fluorescence microscopy by 1.7-fold. Higher resolution 3-dimensional Airyscan images provide a clearer view of TCOF1 foci and the possibility of further data analysis. The volume of foci were measured using Volocity image analysis software (PerkinElmer® Inc., Waltham, MA).

TCOF1 shRNA

Rat TCOF1 shRNA lentiviral particles (Locus ID 291571) containing four unique 29mer target-specific shRNA and one scrambled control shRNA were purchased from OriGene Technologies, Inc. (Rockville, MD) and used according to manufacturer's directions.

Statistical Analysis

Individual comparisons were made using Student's *t* test or analysis of variance (ANOVA) with post hoc Student's Newman-Keul test, as appropriate. Significance was accepted at $P < 0.05$.

RESULTS

Primary cells isolated from the submaxillary gland of the Sprague Dawley rat were X-ray irradiated at a dose range of 2–10 Gy to determine whether radioresistant cells were present. We observed that cells exhibiting an epithelial-like morphology were capable of surviving high radiation doses (5 Gy) (Supplementary Fig. S1; http://dx.doi.org/10.1667/RR15342.1.S1). We began subcloning individual epithelial colonies arising from the clonal expansion of single cells to determine whether the radioresistant phenotype could be isolated *a priori*. Figure 1A shows clonogenic survival for several clonally-derived epithelial cell lines after 5 Gy X-ray irradiation. Cells with high, intermediate and low radioresistance were observed. Three highly radioresistant cell lines (clones 4, 5 and 10) were subjected to microarray analysis to identify the resistant cell type. Clones 4, 5 and 10 expressed mRNA for α-amylase, AQP5 and a number of stem cell markers (*c-Kit*, *Kitlg*, *CD133*, *Abcg2*, *CD24*, *Asc13*, *Aldh1A1* and *LGR5*, among others) (data not shown). Alpha-amylase and AQP5 are indicative of acinar cells (*18*), while the co-expression of stem cell markers suggests that radioresistant cells are acinar progenitors. As confirmation, Western blot analysis was performed to validate the expression of α-amylase, AQP5 and c-Kit in clones 4, 5 and 10 (Fig. 1B). We then examined α-amylase, AQP5 and c-Kit protein expression in cells that survived 10 Gy X-ray irradiation and exhibited long-term proliferative potential, defined by passaging into multiple T75 flasks. Cells surviving 10 Gy X-ray irradiation expressed c-Kit, α-amylase and AQP5 (Fig. 1C), indicating that acinar progenitors were the radioresistant phenotype. Colonies formed by acinar progenitors grow in a circular pattern with no observable cell migration away from the edges (Fig. 1D).

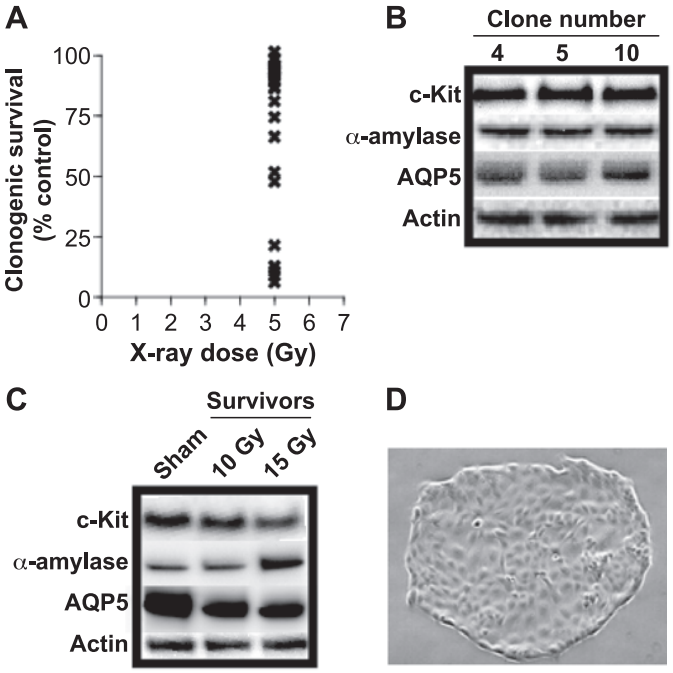

FIG. 1. Identification of acinar progenitor cells as the radiation resistant phenotype. Panel A: Establishment of cell lines with varying degrees of radioresistance via the clonal expansion of single primary cells isolated from the rat submaxillary gland. Panel B: Western blot analysis of c-Kit, α-amylase and AQP5 protein expression in three different radioresistant cell lines indicating an acinar progenitor phenotype. Panel C: Cells surviving 10 Gy X-ray irradiation with long-term proliferative potential retain expression of the progenitor phenotype. Panel D: Representative phase contrast image (20×) of progenitor cell colony. Similar results were observed in at least three separate experiments.

We subsequently characterized acinar progenitors in greater detail. The proliferation rate of progenitors was log-linear, exhibiting a population doubling at ~24-h intervals (Fig. 2A). To achieve this growth rate, either all cells within the colony are dividing at an equal rate or cells at the edge of the colony are dividing at a very rapid rate. The EdU Click-iT assay was used to determine this. Edu is a modified thymidine analog that is incorporated into newly synthesized DNA and is detected by fluorescence microscopy following fluor attachment via click chemistry. Progenitor cells were maintained for several days until large colonies were visible, followed by a 24-h pulse with EdU (i.e., one population doubling). EdU was efficiently incorporated into the DNA of all cells throughout the colony (Fig. 2B). Evidence of mitotic cells was also apparent at the center of the colonies (see arrows for DAPI staining) where cell-cell contact-dependent growth arrest might be expected. These observations indicate that all cells within a colony were dividing at ~24-h intervals. To determine plating efficiency, progenitor cells were seeded at increasing density in 10-cm dishes and colonies were quantified on day 10. Increasing seeded cell number resulted in a linear increase in colony number (Fig. 2C; $r^2 = 0.98$) and plating efficiency was ~50%. We then expanded the radiation

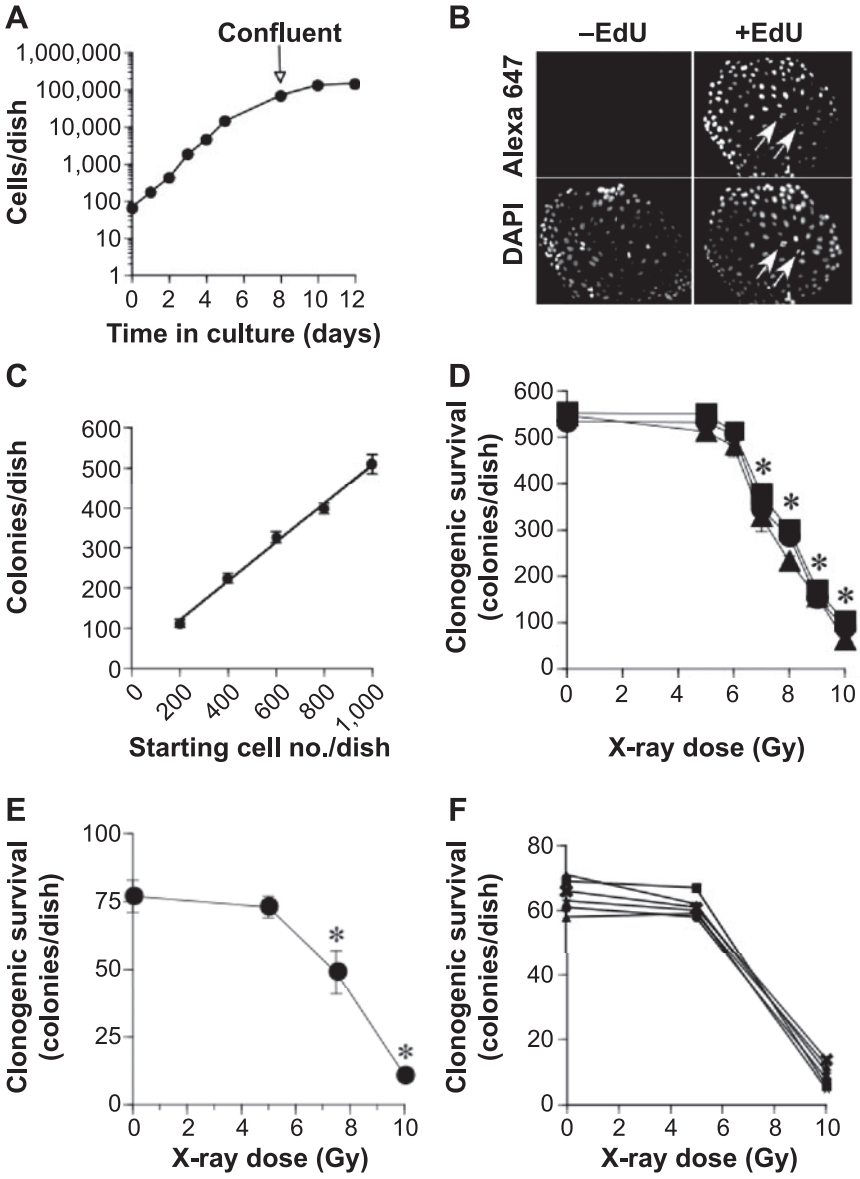

FIG. 2. Progenitor characterization. Panel A: Progenitor cells exhibit a log-linear growth rate with population doubling at ~24-h intervals. Values represent the mean ± standard error (SE) (n = 3). Panel B: A 24-h EdU pulse, encompassing a single population doubling, efficiently labeled the DNA of all cells within a colony. Identical results were observed in three separate experiments. Panel C: Progenitor cells show a linear increase in colony number that parallels plating density ($r^2 = 0.98$), indicating a plating efficiency of ~50%. Values represent the mean ± SE (n = 3). Similar results were observed in two separate experiments. Panel D: Radioresistant progenitor cells received 5–10 Gy X-ray irradiation at passage 5 (square), 10 (circle) or 15 (triangle) and clonogenic survival was quantified as described in Materials and Methods (seeding 1,000 cells/10-cm dish). Values represent the mean ± SE (n = 3). *Significantly different from respective sham-irradiated control.

dose-response analysis and included multiple cell passages using a seeding density of 1,000 cells/10 cm dish to evaluate model stability. The dose-response curve for progenitors at passage 5, 10 and 15 were comparable (Fig. 2D). Because progenitors were highly radioresistant, it was prudent to verify dosimetry. Two different microdosimeters (OSL Nanodots and InLight dosimeters) were placed under a culture dish, which was 10 Gy X-ray irradiated, as described in Materials and Methods. Microdosimeters exposed to 10 Gy X rays registered 9.9 Gy, indicating that the dosimetry was accurate.

The advanced DMEM:F12 media used to culture progenitor cells contains proprietary/undefined components; the possibility that these components were inducing radioresistance was considered. Micronuclei were readily detected 24 h after 5–10 Gy X-ray irradiation of progenitor cells (Fig. 3A and B). Treatment of progenitors with 20 n*M* Ku 55933, an inhibitor of DNA double-strand break repair

(*27*), we observed within the first 6 h after receiving 5 Gy of X rays that there was a dramatic reduction of clonogenic survival (Fig. 3C). These observations indicate that the advanced DMEM was not preventing radiation-induced DNA damage. We then compared clonogenic survival of progenitors and normal human dermal fibroblasts maintained on standard media or after adaptation onto the advanced DMEM:F12 media. Fibroblasts are a radiosensitive phenotype that would be expected to provide sensitive detection of radioresistance induced by the advanced DMEM:F12 media. In both cases, the dose-response curves were essentially identical (Supplementary Fig. S2; http://dx.doi.org/10.1667/RR15342.1.S1). Notably, plating efficiencies of both progenitors and fibroblasts maintained on the advanced DMEM:F12 media were increased compared to standard media (Supplementary Fig. S2). These observations demonstrate that radioresistance was not induced by advanced DMEM:F12.

Based on data shown in Fig. 1A, we suggest that radiosensitive epithelial cells were also present in the initial cellular pool isolated from the submaxillary gland; we sought to determine whether radiosensitive acinar counterparts were present. Figure 4A and B shows two cell lines (clones 18 and 34) with appreciable cell death at X-ray doses ranging from 2–5 Gy, compared to a radioresistant progenitor (clone 10). Alpha-amylase and AQP5 expression were comparable in radiosensitive (clones 18 and 34) and radioresistant (clone 10) cells. In contrast, c-Kit expression was markedly reduced in radiosensitive cells, compared to radioresistant progenitors. Radiosensitive clone 18 and radioresistant clone 10 exhibited stable phenotypes at passages 5–15 (Fig. 4C and D).

The DNA damage response is strongly regulated by protein kinases, and a pilot phosphoproteomics investigation was initiated to determine whether mechanisms of radioresistance could be identified from changes in the radiation phosphoproteome. The experimental design utilized radiosensitive (clone 18) and radioresistant (clone 10) cells, with samples processed 30 min after 5 Gy X-ray irradiation. The phosphopeptide ratio (5 Gy/control) was calculated for each experimental group to identify differences in phosphorylation status of specific phosphopeptides. Supplementary Table S1 (http://dx.doi.org/10.1667/RR15342.1.S2) summarizes the phosphopeptide ratios. We observed that multiple phosphopeptides with 100% homology to the treacle protein (TCOF1), namely S^{792} (SAPVKES*PNKGAYSGTSR) and S^{1254} (QQLAAGTSAGS*PEKASR), exhibited increased phosphorylation in response to radiation in both resistant and sensitive phenotypes. However, radiation induced an approximate doubling of phospho-S^{792} levels in radioresistant, but not radiosensitive cells (1.91 and 1.12, respectively). In contrast, radiation induced an approximate doubling of phospho-S^{1254} levels in both radioresistant and radiosensitive cells (2.13 and 2.02, respectively). This observation suggests that S^{792} phosphorylation is differentially regulated in the radioresistant phenotype. Antibodies against phospho-TCOF1 (S^{792}) are not commercially available, and we used TCOF1 immunoprecipitation in combination with a non-specific phosphoprotein detection method (pIMAGO) to determine whether the phosphorylation status of TCOF1 was increased as

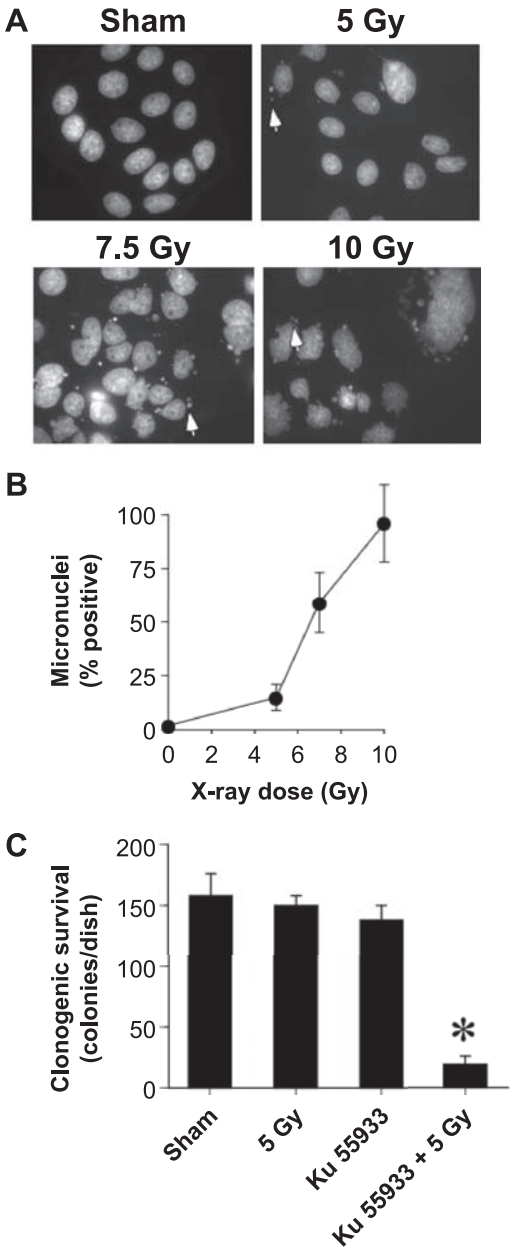

FIG. 3. Evaluation of DNA damage in irradiated progenitor cells. Panel A: Detection of micronuclei (arrows) in progenitor cells X-ray irradiated with 5–10 Gy at 24 h. Panel B: Quantification of radiation-induced micronuclei in progenitor cells. Four independent experiments were pooled to quantify the percentage total cells with detectable micronuclei at 24 h (mean ± SE, n = 4). Panel C: Ku 55933 treatment during the first 6 h postirradiation significantly reduced clonogenic survival of progenitor cells. Values represent the mean ± SE (n = 3). *Significantly different from sham-irradiated control, $P < 0.05$. Similar results were observed in two separate experiments.

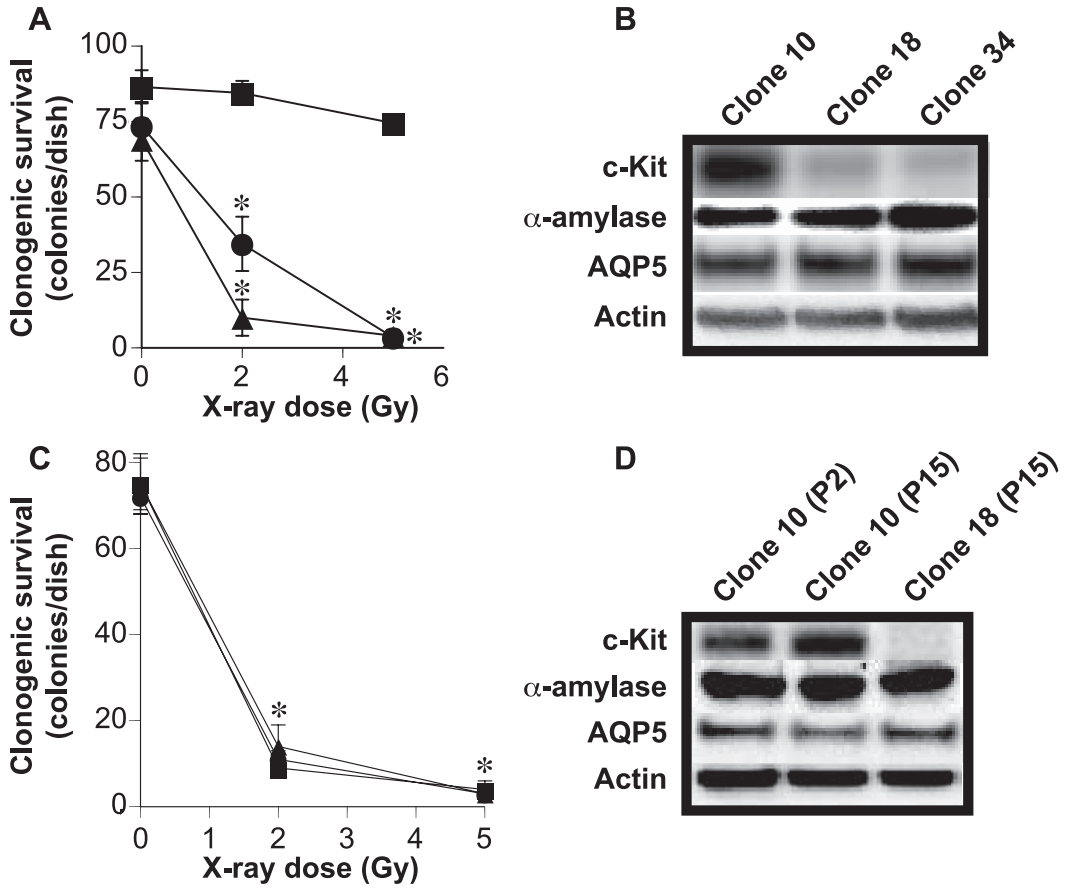

FIG. 4. Isolation of radiosensitive acinar counterparts. Panels A and B: A two-stage screening process was used to identify radiosensitive acinar cells. The first stage identified α-amylase$^+$/AQP5$^+$ cells with sufficient proliferative potential for experimental analysis. The second stage identified the subset of α-amylase$^+$/AQP5$^+$ cells that exhibited reduced clonogenic survival after 2–5 Gy X-ray irradiation. Two clones met these criteria [clone 18 (triangle); clone 34 (circle)] and clonogenic survival for these clones is compared with a radioresistant clone [clone 10 (square)]. Values represent the mean ± SE (n = 3). *Significantly different from respective sham-irradiated control, $P < 0.05$. Panel C: Radiosensitive clone 18 exhibited a stable phenotype at passages 5 (square), 10 (circle) and 15 (triangle). Values represent the mean ± SE (n = 3). Panel D: Radioresistant clone 10 and radiosensitive clone 18 maintain c-Kit, α-amylase and AQP5 expression patterns at passage 15 (P15). *Significantly different from respective sham-irradiated control, $P < 0.05$.

predicted by phosphoproteomics. Figure 5A shows an increase in the phosphorylation status of TCOF1 in both radiosensitive and radioresistant cells 30 min after 5 Gy X-ray irradiation. Interestingly, the phosphorylation status of TCOF1 was disproportionately increased in radioresistant cells compared to radiosensitive counterparts. TCOF1-specific shRNA (lentivirus) was then used to determine whether silencing of TCOF1 expression radiosensitized progenitor cells. Three TCOF1 shRNA constructs were tested and TCOF1 shRNA no. 2 induced the largest decrease in TCOF1 protein levels, as indicated by Western blot (Fig. 5B). TCOF1 shRNA no. 2 and no. 3 decreased clonogenic survival of irradiated progenitor cells (Fig. 5C).

We investigated whether Airyscan super-resolution fluorescence microscopy could provide adequate resolution of subnuclear TCOF1 foci. As expected, TCOF1 was densely packed into nucleosomes in nonirradiated controls; however, the nucleolar localization pattern was dramatically altered in cells surviving 10 Gy X-ray irradiation (Fig. 6A). Using Airyscan, differences in the size of TCOF1 foci could be discerned in sham and 10 Gy irradiated surviving cells (Fig. 6B).

DISCUSSION

Damage to the salivary gland occurs during radiotherapy for head and neck cancers. However, when patients receive lower doses of radiation, salivary gland regeneration can occur. Regeneration of the salivary gland is hypothesized to be mediated by radiation-resistant stem/progenitor cells. c-Kit$^+$ stem/progenitor cells are of particular interest because they are associated with enhanced regenerative potencies in salivary gland models (*16*). With elucidation of the cellular and molecular mechanisms of radioresistance in c-Kit$^+$ salivary gland stem/progenitor cells, it is anticipated that methods will be employed to regulate these mechanisms

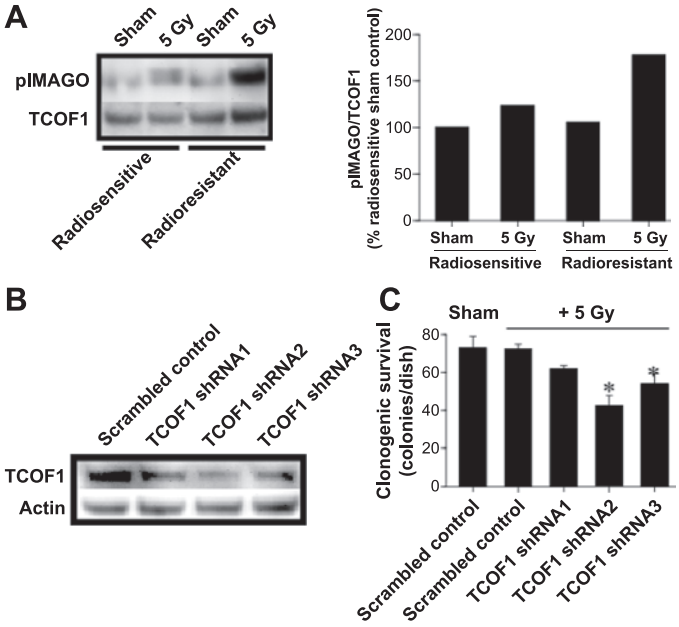

FIG. 5. Identification and functional validation of a role for TCOF1 in progenitor radioresistance. Panel A: The phosphorylation status of TCOF1 was investigated by immunoprecipitation of TCOF1, using the non-specific protein phosphorylation detection method, pIMAGO. An alliquot of the immunoprecipitate was used for TCOF1 Western blot as normalization for the pIMAGO signal. Panel B: Western blot analysis of TCOF1 protein levels in progenitor cells transduced with TCOF1-specific shRNA lentivirus. Panel C: Clonogenic survival of progenitor cells transduced with TCOF1-specific shRNA. Values represent the mean ± SE (n = 3). *Significantly different from sham-irradiated scrambled control shRNA, $P < 0.05$. Similar results were observed in two separate experiments.

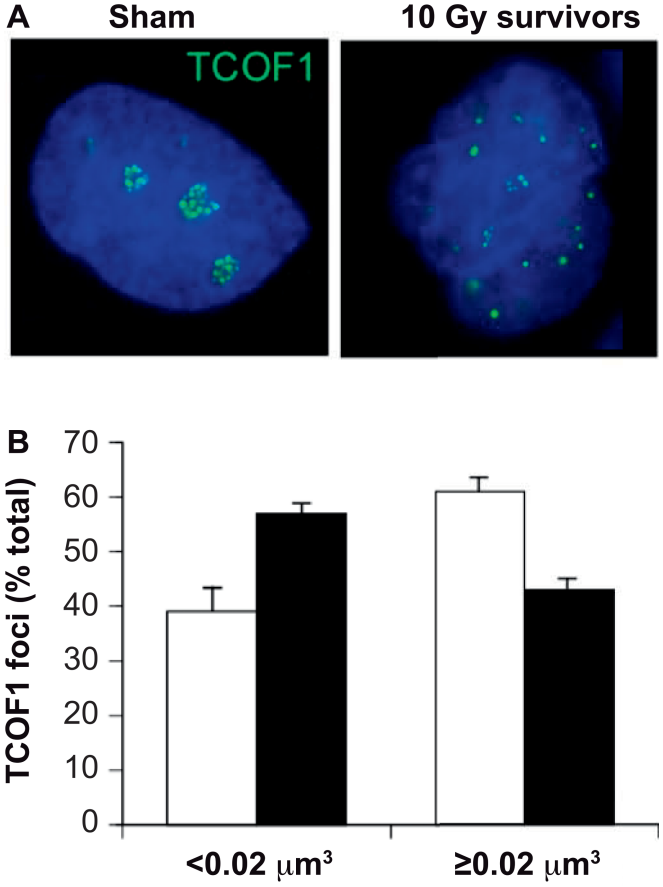

FIG. 6. Disruption of TCOF1 subnuclear localization in cells surviving high-dose irradiation. Panel A: TCOF1 shows predominant nucleolar localization in progenitor cells, but relocalizes throughout the nucleus in cells surviving 10 Gy X-ray irradiation. Panel B: Using Airyscan super resolution fluorescence imaging, the size of TCOF1 foci could be discriminated in control progenitor cells (white), relative to 10 Gy irradiated survivors (black). Values represent the mean ± SE of approximately 100 nuclear foci from multiple cells.

and improve recovery of damaged salivary glands. Rodent models can provide important test systems if molecular mechanisms under investigation are conserved in humans. Our initial characterization demonstrates conservation of TCOF1-mediated radioresistance in human cells (*20*) and c-Kit$^+$ rat progenitor cells (Fig. 5). TCOF1 has the potential to regulate radioresistance at multiple subcellular sites and the stability of rat progenitor cells will enable careful dissection of these sites in future studies.

Our classification of progenitor cells is based on gene expression patterns defined in a transcriptomics analysis and subsequent validation by Western blot. Microarray results indicate that progenitor cells express several stem cell markers (*c-Kit*, *Kitlg*, *CD133*, *Abcg2*, *CD24*, *Ascl3* and *Aldh1A1*, among others) along with differentiation markers for acinar cells (α-amylase, AQP5) (*18*). High expression of c-Kit protein was observed in radioresistant progenitors, while radiosensitive counterparts showed low c-Kit expression (Fig. 4B), consistent with the association of c-Kit with radioresistant phenotypes. c-Kit is interesting because it is implicated in both radioresistance, as well as enhancement of salivary gland regeneration by transplanted stem cells. A number of laboratories have demonstrated that c-Kit$^+$ stem cells/cancer stem cells are radioresistant (*14*) and that inhibiting c-Kit activity can induce apoptosis (*28*) or radiosensitize cancer cell lines (*29*). Thus, the inhibition of apoptosis is one potential mechanism by which c-Kit may promote survival of irradiated stem/progenitor cells. Anti-apoptotic signaling associated with c-Kit expression could also contribute to tissue regeneration by transplanted stem cells. Specifically, stem cells must survive anoikis, a specialized form of apoptosis induced by insufficient matrix support during cell engraftment (*30*). This latter possibility is consistent with reports suggesting that c-Kit expression is associated with enhanced regenerative potencies in salivary gland models (*16*). Additional studies are warranted to decipher the mechanisms by which c-Kit regulates radioresistance and enhances tissue regeneration.

Given the importance of protein kinases in the DNA damage response, we anticipated that phosphoproteomics would reveal mechanisms of radiation resistance in acinar progenitors. In our pilot study, a number of phosphopeptides associated with radioresistance were identified and candidate proteins were inferred based on homology. We elected to investigate the function of TCOF1 in greater

detail due to the potential for TCOF1-dependent radioresistance to be conserved in human cells (*20*). Western blot analysis using the pIMAGO phosphoprotein detection reagent confirmed that the phosphorylation status of TCOF1 was disproportionately increased in irradiated progenitor cells, relative to radiosensitive counterparts (Fig. 5A) consistent with phosphoproteome predictions. Radiation activates the ATM/ATR kinases (*31*), which can phosphorylate TCOF1 on S^{1410}, S^{1411}, S^{1199}, S^{1200}, S^{1216} and S^{1217}, demonstrating that there are many putative radiosensitive phosphorylation sites on TCOF1 that could account for the disproportional increase in TCOF1 phosphorylation. TCOF1-specific shRNA reduced TCOF1 protein levels and radiosensitized progenitor cells (Fig. 5B and C), confirming a functional role for TCOF1 in radioresistance. Independent investigators have demonstrated that silencing TCOF1 (siRNA) sensitizes human cells to genotoxic agents, including radiation (*20*). Therefore, these observations demonstrate that radioresistance associated with TCOF1 is conserved in human and rat cells.

Mechanistically, TCOF1 can form a protein complex with NBS1 in cooperation with ATM to maintain genomic integrity after DNA damage (*20*) and localizes to DNA damage sites (*32*). The size of TCOF1 foci is altered in cells surviving high doses of radiation (Fig. 6B), suggesting altered protein complex formation. Alternatively, TCOF1 localizes to nucleoli (*33*) where it regulates rRNA transcription, pre-RNA processing and ribosomal biogenesis (*34*). Disruption of ribosomal biogenesis can lead to induction of p53 and cell death (*35*). The ribosomal localization of TCOF1 appears to be dramatically altered in progenitor cells surviving high radiation doses (Fig. 6A), which suggests that nucleosome-specific functions of TCOF1 will also be altered. Collectively, TCOF1 is an interesting candidate with multiple functions that could affect radioresistance; additional studies are warranted to determine if one or more TCOF1 functions can be leveraged to alter the survival of irradiated stem/progenitor cells.

We expect that our model system will have multiple applications for identifying new cellular and molecular mechanisms related to the DNA damage response, prosurvival signaling and stem cell biology; however, conservation of such mechanisms in humans remains an important consideration. In one context, prosurvival mechanisms in acinar stem cells might be leveraged to promote the regeneration of damaged salivary gland tissues. There is an immediate need to enhance our understanding of human salivary gland stem cell culture methods to improve stability of the phenotype and longevity of the cultures that limit their translational potential. Rat acinar progenitors exhibit a stable phenotype *in vitro* and identifying the pathways contributing to this stability might enable improvements to human stem cell culture methods. Alternatively, it may also be possible to exploit the pathways promoting radioresistance and prosurvival functions of progenitors to preserve the stem cell niche during radiotherapy of head and neck cancers. These applications will require detailed understanding of conserved mechanisms of action. The stability of our model will enable resolution of mechanisms in detail and the availability of radioresistant and radiosensitive counterparts will contribute to rapid prioritization of targets in global-omic assays. In support of this statement, TCOF1 was readily identified from a very limited pilot effort characterizing the radiation phosphoproteome. A comprehensive analysis of the radiation phosphoproteome is expected to dramatically improve our knowledge of protein kinases and pathways with the potential to regulate radiation resistance and prosurvival signaling. Site-specific phosphorylation patterns can further be interrogated to elucidate their specific effect on target proteins (e.g., control of TCOF1 subcellular distribution and radioresistance). The phosphorylation motifs can aid in identifying the pathways regulating site-specific phosphorylation that may have additional implications in the regulation of radioresistance and prosurvival signaling. Finally, alternative applications of this model may relate molecular mechanisms of radioresistance to the development of new approaches for treating therapeutically-resistant cancers.

SUPPLEMENTARY INFORMATION

Fig. S1. Colony morphologies observed in the clonogenic survival assay.

Fig. S2. Advanced DMEM:F12 does not induce radiation resistance.

Table S1. Raw intensity values for each condition.

ACKNOWLEDGMENTS

This work was supported by the CDC/NIOSH (grant no. RO1 OH008173-06).

Received: January 21, 2019; accepted: May 1, 2019; published online: May 29, 2019

REFERENCES

1. Cancer.net Editorial Board. Head and neck cancer: Statistics. Alexandria, VA: American Society of Clinical Oncology; 2019. (https://bit.ly/2GXPiWi)
2. Grundmann O, Mitchell GC, Limesand KH. Sensitivity of salivary glands to radiation: from animal models to therapies. J Dent Res 2009; 88:894–903.
3. Hancock PJ, Epstein JB, Sadler GR. Oral and dental management related to radiation therapy for head and neck cancer. J Can Dent Assoc 2003; 69:585–90.
4. Cady J. Nutritional support during radiotherapy for head and neck cancer: the role of prophylactic feeding tube placement. Clin J Oncol Nurs 2007; 11:875–80.
5. Nguyen NP, Vos P, Karlsson U, Nguyen P, Dutta S, Lemanski C, et al. Quality of life following chemoradiation and postoperative radiation for locally advanced head and neck cancer. Otorhinolaryngol Relat Spec 2007; 69:271–6.
6. Hall E. Radiobiology for the radiologist. 5th ed. Philadelphia: Lippincott, Williams and Wilkins; 2000.
7. Henson BS, Eisbruch A, D'Hondt E, Ship JA. Two-year longitudinal study of parotid salivary flow rates in head and neck

cancer patients receiving unilateral neck parotid-sparing radiotherapy treatment. Oral Oncol 1999; 35:234–41.

8. Robar JL, Day A, Clancey J, Kelly R, Yewondwossen M, Hollenhorst H, et al. Spatial and dosimetric variability of organs at risk in head-and-neck intensity-modulated radiotherapy. Int J Radiat Oncol Biol Phys 2007; 68:1121–30.
9. Hoebers FJ, Kartachova M, de Bois J, van den Brekel MW, van Tinteren H, van Herk M, et al. 99mTc Hynic-rh-Annexin V scintigraphy for in vivo imaging of apoptosis in patients with head and neck cancer treated with chemoradiotherapy. Eur J Nucl Med Mol Imaging 2008; 35:509–18.
10. Eisbruch A, Kim HM, Terrell JE, Marsh LH, Dawson LA, Ship JA. Xerostomia and its predictors following parotid-sparing irradiation of head-and-neck cancer. Int J Radiat Oncol Biol Phys 2001; 50:695–704.
11. Dirix P, Nuyts S, Van den Bogaert W. Radiation-induced xerostomia in patients with head and neck cancer: a literature review. Cancer 2006; 107:2525–34.
12. Braam PM, Terhaard CH, Roesink JM, Raaijmakers CP. Intensity-modulated radiotherapy significantly reduces xerostomia compared with conventional radiotherapy. Int J Radiat Oncol Biol Phys 2006; 66:975–80.
13. Dingwall S, Lee JB, Guezguez B, Fiebig A, McNicol J, Boreham D, et al. Neoplastic human embryonic stem cells as a model of radiation resistance of human cancer stem cells. Oncotarget 2015; 6:22258–69.
14. Perez-Losada J, Sanchez-Martin M, Perez-Caro M, Perez-Mancera PA, Sanchez-Garcia I. The radioresistance biological function of the SCF/kit signaling pathway is mediated by the zinc-finger transcription factor Slug. Oncogene 2003; 22:4205–11.
15. Lombaert IM, Brunsting JF, Wierenga PK, Faber H, Stokman MA, Kok T, et al. Rescue of salivary gland function after stem cell transplantation in irradiated glands. PloS One 2008; 3:e2063.
16. Pringle S, Maimets M, van der Zwaag M, Stokman MA, van Gosliga D, Zwart E, et al. Human salivary gland stem cells functionally restore radiation damaged salivary glands. Stem Cells 2016; 34:640–52.
17. Maimets M, Rocchi C, Bron R, Pringle S, Kuipers J, Giepmans BN, et al. Long-term in vitro expansion of salivary gland stem cells driven by Wnt signals. Stem Cell Rep 2016; 6:150–62.
18. Weber TJ, Smith JN, Carver ZA, Timchalk C. Non-invasive saliva human biomonitoring: development of an in vitro platform. J Expo Sci Environ Epidemiol 2017; 27:72–7.
19. Carver ZA, Han AA, Timchalk C, Weber TJ, Tyrrell KJ, Sontag RL, et al. Evaluation of non-invasive biomonitoring of 2,4-Dichlorophenoxyacetic acid (2,4-D) in saliva. Toxicology 2018; 410:171–81.
20. Ciccia A, Huang JW, Izhar L, Sowa ME, Harper JW, Elledge SJ. Treacher Collins syndrome TCOF1 protein cooperates with NBS1 in the DNA damage response. Proc Natl Acad Sci U S A 2014; 111:18631–6.
21. Wright AT, Magnaldo T, Sontag RL, Anderson LN, Sadler NC, Piehowski PD, et al. Deficient expression of aldehyde dehydrogenase 1A1 is consistent with increased sensitivity of Gorlin syndrome patients to radiation carcinogenesis. Mol Carcinog 2015; 54:473–84.
22. Weber TJ, Magnaldo T, Xiong Y. ALDH1A1 Deficiency in Gorlin syndrome suggests a central role for retinoic acid and ATM deficits in radiation carcinogenesis. Proteome 2014; 2:451–67.
23. Ficarro SB, Adelmant G, Tomar MN, Zhang Y, Cheng VJ, Marto JA. Magnetic bead processor for rapid evaluation and optimization of parameters for phosphopeptide enrichment. Anal Chem 2009; 81:4566–75.
24. Kim S, Mischerikow N, Bandeira N, Navarro JD, Wich L, Mohammed S, et al. The generating function of CID, ETD, and CID/ETD pairs of tandem mass spectra: applications to database search. Mol Cell Proteomics 2010; 9:2840–52.
25. Qian WJ, Liu T, Monroe ME, Strittmatter EF, Jacobs JM, Kangas LJ, et al. Probability-based evaluation of peptide and protein identifications from tandem mass spectrometry and SEQUEST analysis: the human proteome. J Proteome Res 2005; 4:53–62.
26. Polpitiya AD, Qian WJ, Jaitly N, Petyuk VA, Adkins JN, Camp DG, 2nd, et al. DAnTE: a statistical tool for quantitative analysis of -omics data. Bioinformatics 2008; 24:1556–8.
27. Teng PN, Bateman NW, Darcy KM, Hamilton CA, Maxwell GL, Bakkenist CJ, et al. Pharmacologic inhibition of ATR and ATM offers clinically important distinctions to enhancing platinum or radiation response in ovarian, endometrial, and cervical cancer cells. Gynecol Oncol 2015; 136:554–61.
28. Stankov K, Popovic S, Mikov M. C-KIT signaling in cancer treatment. Curr Pharm Des 2014; 20:2849–80.
29. Eberle F, Leinberger FH, Saulich MF, Seeger W, Engenhart-Cabillic R, Hanze J, et al. In cancer cell lines inhibition of SCF/c-Kit pathway leads to radiosensitization only when SCF is strongly overexpressed. Clin Transl Radiat Oncol 2017; 2:69–75.
30. Chae DS, Lee CY, Lee J, Seo HH, Choi CH, Lee S, et al. Priming stem cells with protein kinase C activator enhances early stem cell-chondrocyte interaction by increasing adhesion molecules. Biol Res 2018; 51:41.
31. Matsuoka S, Ballif BA, Smogorzewska A, McDonald ER 3rd, Hurov KE, Luo J, et al. ATM and ATR substrate analysis reveals extensive protein networks responsive to DNA damage. Science 2007; 316:1160–6.
32. Sakai D, Trainor PA. Face off against ROS: Tcof1/Treacle safeguards neuroepithelial cells and progenitor neural crest cells from oxidative stress during craniofacial development. Dev Growth Differ 2016; 58:577–85.
33. Brown DD, Gurdon JB. Absence of ribosomal RNA synthesis in the anucleolate mutant of Xenopus Laevis. Proc Natl Acad Sci U S A 1964; 51:139–46.
34. Valdez BC, Henning D, So RB, Dixon J, Dixon MJ. The Treacher Collins syndrome (TCOF1) gene product is involved in ribosomal DNA gene transcription by interacting with upstream binding factor. Proc Natl Acad Sci U S A 2004; 101:10709–14.
35. Rubbi CP, Milner J. Disruption of the nucleolus mediates stabilization of p53 in response to DNA damage and other stresses. EMBO J 2003; 22:6068–77.